Electronic supplementary Information (ESI†)

Mesoporous Nanomagnet Supercaptors for Selective Heme-proteins from Human Cells

M. Khairy, Sherif A. El-Safty*, M. Ismael

National Institute for Materials Science (NIMS), 1-2-1 Sengen, Tsukuba-shi, Ibaraki-ken, 305-0047, Japan.

Graduate School for Advanced Science and Engineering,, Waseda University, 3-4-1 Okubo, Shinjuku-ku, Tokyo.169-8555, Japan.

Tel:+81-298592135; Fax: +81-298592025

E-mail: sherif.elsafty@nims.go.jp; sherif@aoni.waseda.jp

Supplementary S1:

i)   Materials.

All materials were used without further purification. Nickel chloride, anhydrous sodium acetate (NaAc), ferric chloride, ferrous chloride, ammonia solution, Ethylene glycol (EG), and oleic acid were obtained from Wako Company Ltd. Osaka, Japan. Polyethyleneimine, Insulin (Ins, 5.733 kDa, 2.4 nm), Cytochrome C (CytC, 12,327 kDa, 3.0 nm), Myoglobin (Mb, 16,950 kDa, 4.0 nm), α-Amylase (α-Amy, ~54 kDa, 6.8 nm), Hemoglobin (Hb, 68.000 kDa, 7.0 nm), and Myosin (My, 200-500 kDa, ~14–19 nm) were obtained from Sigma-Adrich Company Ltd., USA.

ii)   Fabrication of nanocaptors.

The NiO and Fe_3O_4 nanostructures were synthesized via a simple and one-pot hydrothermal method.

Fabrication of magnetic mesoporous NiO NRs.

In a typical synthesis, 2.7 g of anhydrous nickel chloride precursor and 4.5 g of anhydrous sodium acetate (NaAc) were dissolved in 80 mL of Ethylene glycol (EG), followed by 1 g polyethyleneimine, which were then mixed via sonication to achieve a clear solution. The solution was loaded into a 100 mL Teflon-lined, stainless steel autoclave, which was then sealed and maintained at 200 °C for 6 h. Subsequently, the solution was allowed to cool at room temperature. The precipitate was then collected and washed several times with distilled water and ethanol to remove the remaining agents, and was dried at 45 °C. Finally, the NiO

powder was calcined at 270 °C for 30 min with a heating rate of 2 °C/min based on TG and DTA analysis (see Figure S1*).*

Fabrication of magnetic mesoporous NiO NPLs.

Approximately 2.58 g of nickel chloride hexahydrate precursor and 3.2 g of anhydrous NaAc were dissolved in a mixture of 40 mL of EG and 10 mL de-ionized water. The solution was loaded in a 100 mL Teflon-lined, stainless steel autoclave, which was then sealed and maintained at 200 °C for 6 h. Subsequently, the solution was allowed to cool at room temperature. The precipitate was then collected and washed several times with distilled water and ethanol to remove the remaining agents, and was dried at 45 °C. The NiO powder was calcined at 270 °C for 2 h with a heating rate of 2 °C/min.

Fabrication of magnetic mesoporous NiO NSs.

Approximately 1.47 g of nickel chloride precursor and 4.5 g of NaAc was dissolved in 25 mL triethanol amine and 50 mL de-ionized H_2O. Subsequently, 2 g of polyethyleneimine was added. The solution was transferred to a 100 mL Teflon-lined, stainless steel autoclave, which was sealed, and maintained at 200 °C for 8 h. The solution was then allowed to cool at room temperature. The precipitate was collected and washed several times with distilled water and ethanol to remove the remaining agents, and then dried at 45 °C. The NiO powder was calcined at 270 °C for 30 min with a heating rate of 2 °C/min.

Fabrication of anti-ferromagetic mesoporous NiO NPLs.

The anti-ferromagetic mesoporous NiO NPLs were prepared according the reported method of El-Safty group's.[6a] Approximately 10.0 mmoles anhydrous nickel chloride was dissolved

in a mixture of 50 mL distilled water and EG. The solution pH was adjusted to 10 through drop-wise addition of ammonia solution (28%). Subsequently, the solution was loaded into the Teflon liner of a stainless steel autoclave with a volume of 100 mL, which was then sealed and maintained at 160 °C for 6 h. The solution was allowed at cool to room temperature. Finally, the precipitate was collected and washed several times with distilled water and ethanol to remove the remaining agents. After which, the precipitate was dried at 45 °C overnight and carefully calcined at 300 °C in a quartz tube furnace for 2 h with a heating rate of 2 °C/min.
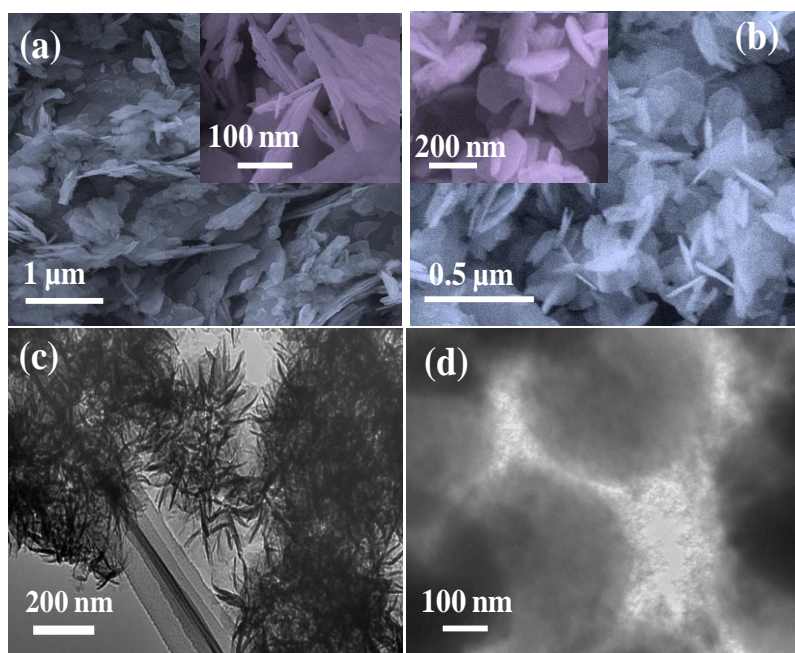
Figure S1 The FE-SEM and TEM profiles of NiO NPs, a) NiO NPLs (rectangular), b)NiO NPLs (Hexagonal), c)NiO NRs, and d) NiO NSs

Supplementary S2:

Thermal decomposition of mesoporousNiO NMs

The thermal decomposition of sample moieties of NRs, NPLs, and NSs (Figure S1) was revealed using thermogravimetry-differential thermal analysis (TG-DTA) techniques. The TG profile (Fig. S1) reveals that the solid sample decreased in mass at around 270 °C to 340 °C. This decrease was accompanied by an endothermic peak in the corresponding DTA curve, indicating the decomposition of the organic moieties. The weight loss from the decomposition process was 25.8%, 27.5%, and 28.447% wt for NRs, NPLs, and NSs, respectively.
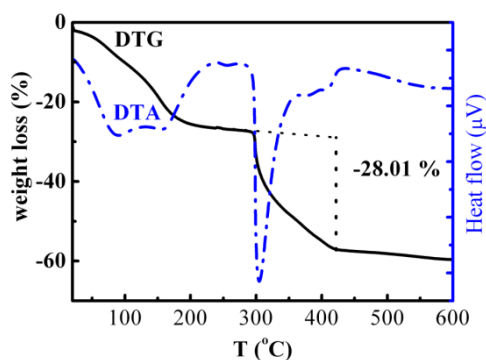
Figure S2. DTG and DTA profiles of NiO NSs.

Supplementary S3:

Fabrication of magnetic mesoporous Fe$_3$O$_4$ NPs. [3c, 4a]

Approximately 9.6 g of ferric chloride hexahydrate and 4 g of ferrous chloride tetrahydrate were dissolved in 30 mL H$_2$O, followed by the addition of 1.7 mL Oleic acid. The solution was then heated at 90 °C, and then 40 mL NH$_4$OH (14%) was added. Subsequently, the temperature was maintained at 90 °C for 5 h. The precipitate was then collected and washed several times with distilled water and ethanol to remove the remaining agents, and dried at 45 °C overnight.
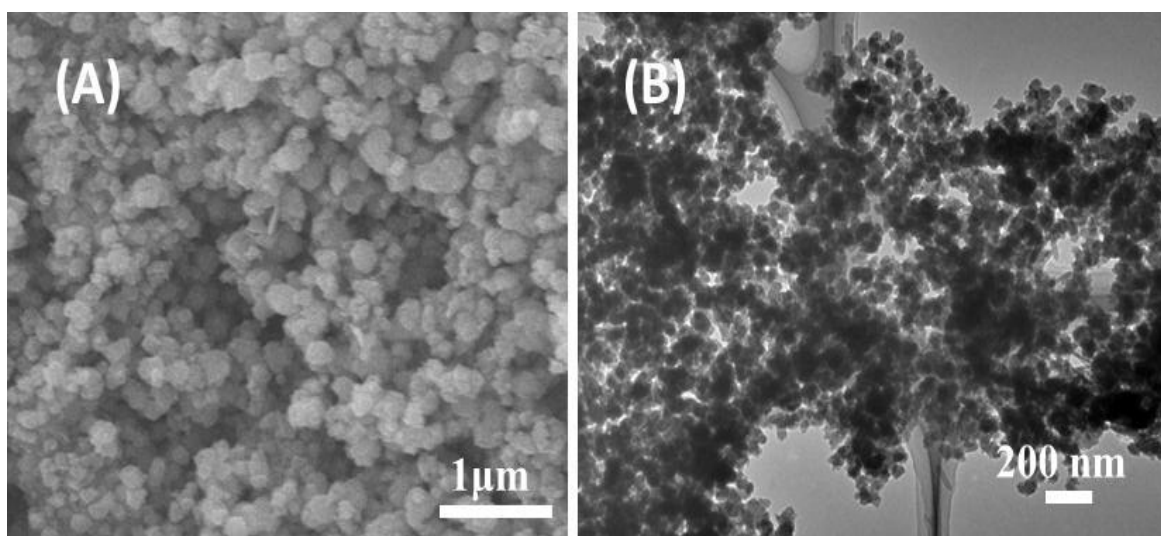
Figure S3. (A) SEM image and TEM micrograph (B) of mesoporous Fe$_3$O$_4$ NPs

Supplementary S4:

Characterization of the NiO NMs

The textural surface properties of the mesoporous NiO or Fe_3O_4 NPs including the specific surface area and the pore structure were determined by N_2 adsorption-desorption isotherms which were measured using a BELSORP MIN-II analyzer (JP. BEL Co. Ltd) at 77 K. The pore size distribution was determined from the adsorption isotherms by using nonlocal density functional theory (NLDFT). Specific surface area (S_{BET}) was calculated using multi-point adsorption data from linear segment of the N_2 adsorption isotherms using Brunauer-Emmett-Teller (BET) theory. Before the N_2 isothermal analysis, all samples were pre-treated at 200 ^{o}C for 3h and calibrated to 10^{-3} Torr.

The morphologies of the NiO samples were investigated via field emission scanning electron microscopy (FE-SEM, JEOL model 6500). Before insertion into the chamber, the NiO or Fe_3O_4 powders were grinded and fixed onto a specimen stub using a 1double-sided carbon tape. Then, a 10 nm Pt film was coated via anion sputtering (Hitachi E-1030) at room temperature to obtain high-resolution micrographs. Before sputtering deposition, the Pt target (4 in diameter, purity 99.95%) was sputter cleaned in pure Ar. The sputtering deposition system used for the experiments consists of a stainless steel chamber, evacuated down to 8×10^{-5} Pa with a turbo molecular pump backed up by a rotary pump. The Ar working pressure (2.8×10^{-1} Pa), the power supply (100 W), and the deposition rate were kept constant throughout these investigations. Moreover, to record the SEM micrographs of the Ni samples better, the scanning electron microscope was operated at 20 keV.

High-resolution transmission electron microscopy (HRTEM), electron diffraction (ED), scanning transmission electron microscopy (STEM), and energy dispersive X-ray spectroscopy for elemental mapping (STEM-EDS) were performed using a JEOL JEM model 2100F microscope. HRTEM was conducted at an acceleration voltage of 200 kV to obtain a lattice resolution of 0.1 nm. The HRTEM micrographs were recorded using a CCD camera. STEM and STEM-EDS were carried out at a camera length of 40 cm and a spot size of 1 nm. In the HRTEM, ED, STEM, and STEM-EDS characterization, the NiO or Fe_3O_4 sample was dispersed in ethanol solution using an ultrasonic cleaner, and then dropped on a copper grid. Prior to inserting the samples into the HRTEM column, the grid was vacuum dried for 20 min.

X-ray photoelectron spectroscopy (XPS) was conducted using a PHI Quantera SXM (ULVAC-PHI) (Perkin–Elmer Co., USA) with monochromated AlKα radiation (1.5 × 0.1 mm, 15 kV, 50 W).

Small angle X-ray scattering (SAXS) experiments were performed at room temperature. A two-dimensional (2D) confocal mirror (Rigaku Nanoviewer) and a pinhole collimator were used to obtain a focused high flux/high transmission; a monochromatic X-ray beam of CuKα radiation (λ = 1.54 Å) was also used. The 2D SAXS patterns were recorded using a 2D detector (BrukerHi-Star) covering a range of momentum transfer $q = (4\pi/\lambda)\ sin(2\theta/2)$, from 0.2 to 10 cm^{-1}, where λ is the wavelength of the incident X-ray beam and 2θ is the scattering angle. The value of inter-particle distance (center to center) was calculated from $d = 2\pi\ /\ q_{max}$.

Wide-angle powder X-ray diffraction (XRD) patterns were measured using an 18 kW diffractometer (Bruker D8 Advance) with monochromated Cu Ka radiation. The sample measurement was repeated three times under rotation at various angles (15°, 30°, and 45°).

The diffraction data were analyzed using the DIFRAC plus Evaluation Package (EVA) software with the PDF-2 Release 2009 databases provided by Bruker AXS. The standard diffraction data were identified according to the databases of the International Centre for Diffraction Data (ICDD). For poor quality diffraction data, the TOPAS package program provided by Bruker AXS 2009 for profile and structure analysis was applied to integrate various types of X-ray diffraction analyses by supporting all profile fit methods currently employed in powder diffractometry.

The magnetic properties were measured with a Quantum Design MPMS superconducting quantum interferometer device (SQUID) magnetometer with an applied magnetic field of up to 70 kOe at 300 K.

The absorbance spectrum of the adsorption process was recorded using a UV-vis spectrophotometer model a Shimadzu 3700 model solid-state, Japan.

The microscopic image of adsorption of hemoglobin blood at NiO or Fe_3O_4 surface was evaluated using Olympus system microscope model BX53. The image is illumined using filter excitation BP 460-495, mirror unit is U-FBW, and barrier filter is BAS101F.

Supplementary S5:

The Batch adsorption method of proteins over nanoscale materials

The biosorbent based on NiO and Fe_3O_4 nanostructured materials were used for the separation of proteins such as hemoglobin (Hb), myoglobin (Mb) and cytochrome c (CytC), insulin (Ins), α-amylase (Amy), and myosin (My) respectively. In such a batch adsorption experiment, (0.025 g) NiO and Fe_3O_4 nonmaterials were performed in an aqueous solution (30 ml deionized water) under constant stirring conditions and at different temperatures (20 °C to 35 °C, ± 0.1 °C range). The initial concentration used of proteins was in the range of 3.5 x 10^{-6} mol. dm^{-3} to 6.01 x 10^{-5} $mol.dm^{-3}$. Afterwards, the aliquot protein was collected and monitored as a function of adsorption time. The concentration of Hb, Mb, CytC, Ins, Amy, and My proteins were studied using UV−vis spectroscopy (a Shimadzu 3700 model solid-state) at λ of 277, 409, 408, 405, 252 and 267 nm, respectively. The decrease of the UV-vis spectra of all proteins at specific wavelengths indicated the adsorbed amount of proteins within these adsorption processes. Basically, hemoglobin is a quaternary protein that occurs in the red blood cells, whereas, myoglobin and cytochrom C were a tertiary protein found in the muscle cells, and liver cells of mammals, respectively.

i) *The Molecular weight and size of proteins:*

Protein	M.wt (g/mol)	Size (nm)
insulin	5733	2.4
α-Amylase	58000	6.8 nm
Myosin	220000	14nm
Cytochrome c	12327	2.5 x 2.5 x 3.7 nm
myoglobin	16950	2.5 × 3.5 ×4.5 nm
hemoglobin	68000	7.0 nm

The percentage of adsorbed amounts (X) of proteins at steady state was calculated by the following equation (1):

$$\%X = (q_f/q_o) \times 100 \qquad (1)$$

Where q_f is the adsorbed quantity of the proteins (Ins, CytC, Mb, Hb, Amy, and My) at steady state, and q_o is the maximum amount of protein when the adsorbed time is equal to affinity

The adsorbed amounts (q_f, mmol. g^{-1}) of the protein molecules at the steady state (equilibrium step), in which the protein was covered the nanoparticle surfaces, was determined according to the equation (2):

$$q_f = (C_o - C_f) \, V/m \qquad (2)$$

Where q_f is the adsorbed amount at steady state, V is the solution volume (L), m is the mass of biosorbent (g), C_o and C_f are the initial concentration and the concentration at saturation time t, respectively.

The adsorption characteristics of protein molecules onto the adsorbents can be studied through the Langmuir adsorption isotherm equation as follows:

$$\frac{C_e}{q_e} = \frac{1}{K_L q_m} + \left(\frac{1}{q_m}\right) C_e \qquad (3)$$

Where q_m (μmol g^{-1}) is the amount of protein molecules adsorbed to form a monolayer coverage, and K_L is Langmuir adsorption equilibrium constants. From the plot of C_e/q_e against C_e, q_m, and K_L can be determined from the slope and the intercept.

The intra-particle diffusion of proteins into nanomagnets can be determined by;

11

$$q_t = kt^{0.5} + C \qquad (5)$$

Where k is the intra-particle diffusion rate constant and C is the intercept which indicates the boundary layers thickness. q_t is the adsorbed quantity of protein molecule at time (t).

The batch adsorption of proteins into nanomagnets was analyzed by applying Lagergren's equation:

$$\frac{dq}{dt} = k_t(q_e - q_t) \qquad (6)$$

By applying the initial conditions $q_t = 0$ at $t = 0$, the linear integration form of pseudo first order model can be expressed as:

$$Ln \left({}^{q_e - q_t}/_{q_e} \right) = K_t t \qquad (7)$$

where k_t is the rate constant (per gram adsorbent, pga) of the first-order kinetics. The free energy of the activation ($\Delta G^{\#}$), the enthalpy of activation ($\Delta H^{\#}$) and the entropy of activation ($\Delta S^{\#}$) were calculated from Eyring's equation:

$$k_t = \frac{KT}{h} e^{-\Delta G^{\#}/RT} \qquad (8)$$

$$\Delta H^{\#} = E - RT \qquad (9)$$

$$\Delta G^{\#} = \Delta H^{\#} - T\Delta S^{\#} \qquad (10)$$

$$Ln \, {}^{k_t h}/_{KT} = {}^{-\Delta H}/_{RT} + {}^{\Delta S}/_{R} \qquad (11)$$

Where k is Boltzmann's constant, h is Planck's constants and T is absolute temperature. The thermodynamic equilibrium constant, K_c which is dependent upon the fractional attainment of equilibrium (f_e) of the protein adsorbed molecules deduced from the following equation:

$$K_c = {q_f}/{(1 - q_f)} \qquad (12)$$

Where q_f is the ratio of the amount of molecule adsorbed at a time (q_t) to that adsorbed at infinity (q_∞), (i.e. $q_f = q_t / q_\infty$).

From the value of K_c, the Gibbs free energy change, ΔG, can be derived. The plot of ln K_c vs. $1/T$, gives the numerical values of ΔH of the adsorption of protein adsorption; ΔG and ΔS using the following relations:

$$\Delta G = -RTLnK_c \qquad (13)$$

$$Ln\,K_c = -{\Delta H}/{RT} + {\Delta S}/{R} \qquad (14)$$

Where ΔH, ΔS, ΔG, and T are the change in enthalpy, the change in entropy, the change in Gibbs free energy and temperature in kelvin, respectively. R is the gas constant and K_c is equilibrium constant.

Supplementary S6:

The STEM and STEM-EDS mapping for NiO NMs were carried out. Our finding reveal that NiO NRs were formed having diameters of ~250 nm, with uniformly distributed Ni and O atoms in the hierarchical rose structure. The Ni and O were originally found in NiO NCs with rose-like morphology, having a [Ni] / [O] ratio of 1.1, which indicates slightly deficient O atoms on the surface. The STEM and STEM-EDS mapping of NiO NSs and NiO NPLs revealed the formation of nanostructures with a size of 500 nm and 50 nm, respectively. The uniform distribution of Ni and O atoms over the NiO NPs and the [Ni]/[O] ratio is about 1.4. This result indicates the formation of rich Ni particles and slightly deficient of O atoms on the surface.
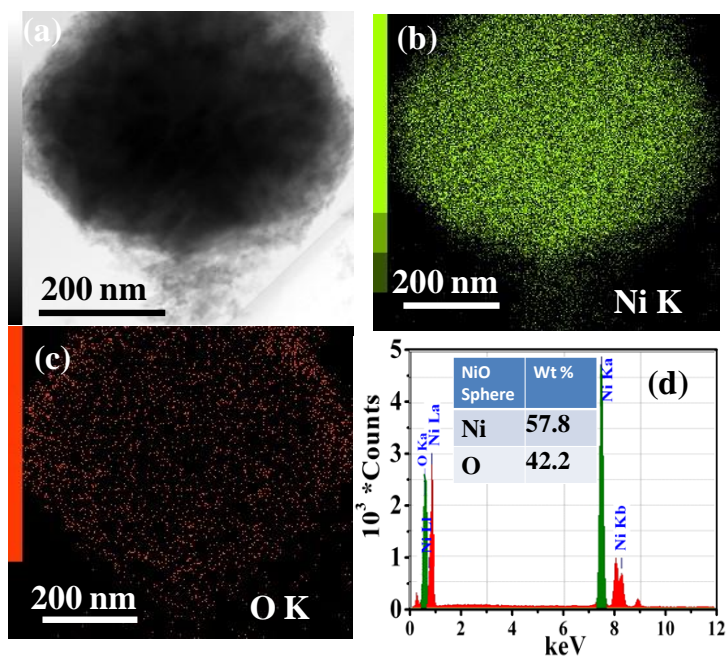
Figure S6. STEM-EDS mapping and EDS analysis of the NiO sphere a) STEM image, b) Nickel, c) Oxygen and d) the calculated values of atomic abundance of Ni, and O atomic present in the NiO sphere.

Supplementary S7:
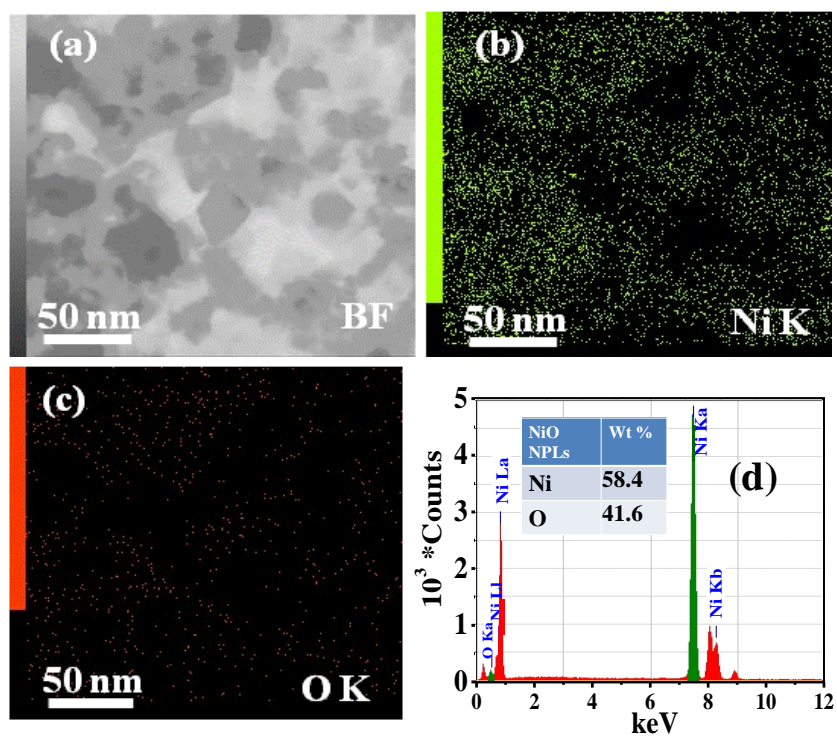
Figure S7. STEM-EDS mapping and EDS analysis of the NiO nanoplatelets a) STEM image, b) Nickel, c) Oxygen d) the calculated values of atomic abundance of Ni, and O atomic species present in the NiO platelets.

Supplementary S8:

The small-angle X-ray scattering (SAXS) profiles of the NiO NPs and Fe_3O_4 NPs were subjected to absolute intensity scaling after normalizing the in-plane diffracted beams with substrate thickness. The scattering intensity and peak resolution in the range of $1.3 < q < 2.2$ strongly suggests that the mesostructures with a degree of mesoporosity could be formed within NiO NMs. The typical X-ray diffraction patterns of the NiO NMs are consistent with the face-centered cubic Fm3m symmetry with a lattice constant a = 4.194 Å (JCPDS, No. 01-089-7130).
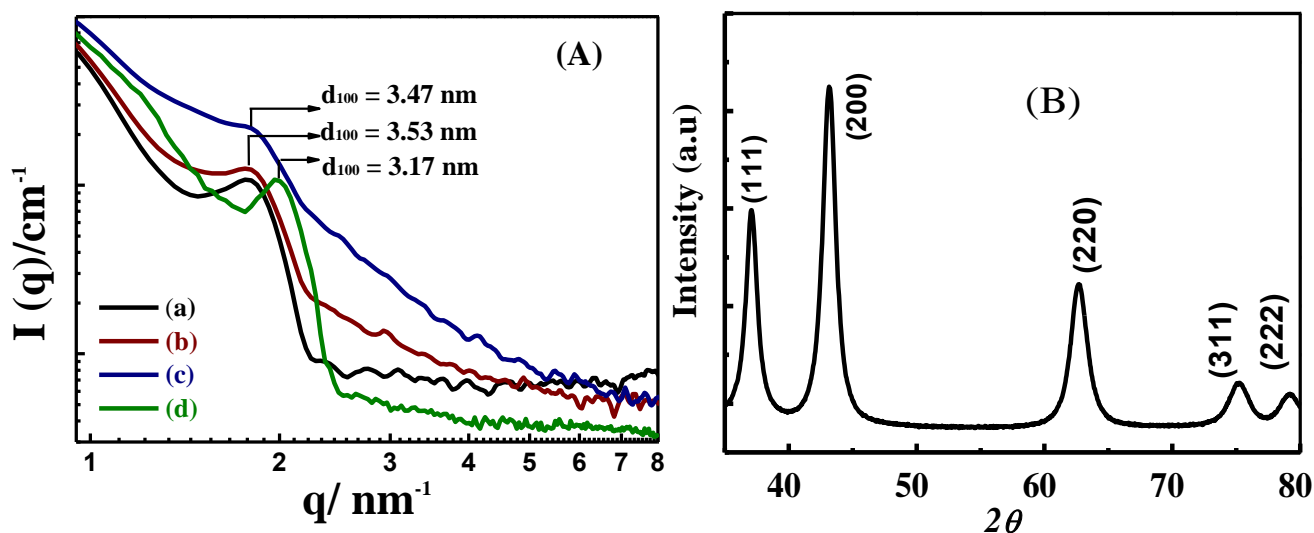
Figure S8. A) SAXS pattern of mesoporous NiO NMs a) nanoroses, b) nanospheres, c) nanoplatelets and c) nanoplatelets and Fe_3O_4 NPs. B) Wide angle X-Ray diffraction of mesoporous NiO NMs

Supplementary S9

The N_2 isotherms of the NiO NFs and NSs featured the type IV isotherms with an H_2-type hysteresis loop for typical mesocage materials with large pore cavities (10 nm to 30 nm).[11] Whereas, NiO NPLs (rectangular), demonstrates type II isotherm with bimodal pore size 30 nm and 280 nm. This finding demonstrates that the synthesis protocol provides effective control over the size and shape of cage opening and cavity pores. The specific surface area was $S_{BET} = 115.7$ m^2g^{-1}, 60.1 m^2g^{-1}, and 45.2 m^2g^{-1} for NiO NRs, NSs, and NPLs, respectively. In addition the N_2 adsorption/ desoption isotherm of Fe_3O_4 NPs reveals high porosity with specific surface area ($S_{BET} = 51.36$ m^2g^{-1}) and bimodal pore size (5.8nm to 60 nm).
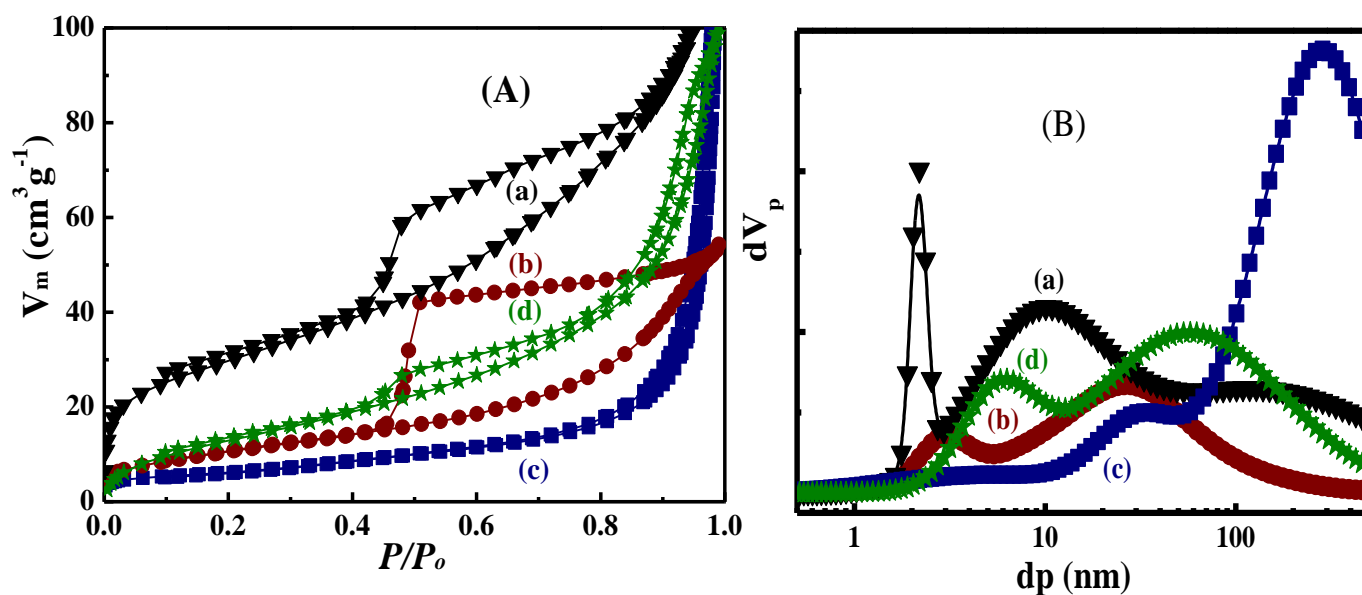
Figure 9 N_2 adsorption isotherms of A) mesoporous NiO a) nanoroses, b) nanospheres, and c) nanoplatelets and Fe_3O_4 NPs (d), B) NLDFT profile of the pore size distribution of mesoporous NiO nanomagnet.

Supplementary S10

When the dimensions of anti-ferromagnetic oxides are decreased to a nanoscale, a variety of new physical phenomena was exhibited, including weak ferro-magnetism and para-magnetism arising from the surface and finite size effects or net magnetic moment coming from uncompensated spins. This surface effect was studied by Něel in 1961, when he suggested that small particles of an anti-ferromagnetic oxide should exhibit super para-magnetism and weak ferro-magnetism. This phenomenon is attributed to the permanent magnetic moment to uncompensated spins in the two sub-lattices. The number of uncompensated spins (q) depends on the crystal structure and particle morphology, and three different models were considered. If the uncompensated spins are randomly distributed in the particle, it is expected that $q \, \alpha \, n_S^{1/2}$ (where n_S is the total number of spins). However, if they are arranged parallel to each other in an odd number of layers stacked in a cube, then $q \, \alpha \, n_S^{2/3}$. Finally, if the core of the particles has no defects, and the uncompensated moments are randomly distributed at the surface, then $q \, \alpha \, n_S^{1/3}$. The unexpected magnetic behavior of NiO NPs largely depends on their synthetic methods.
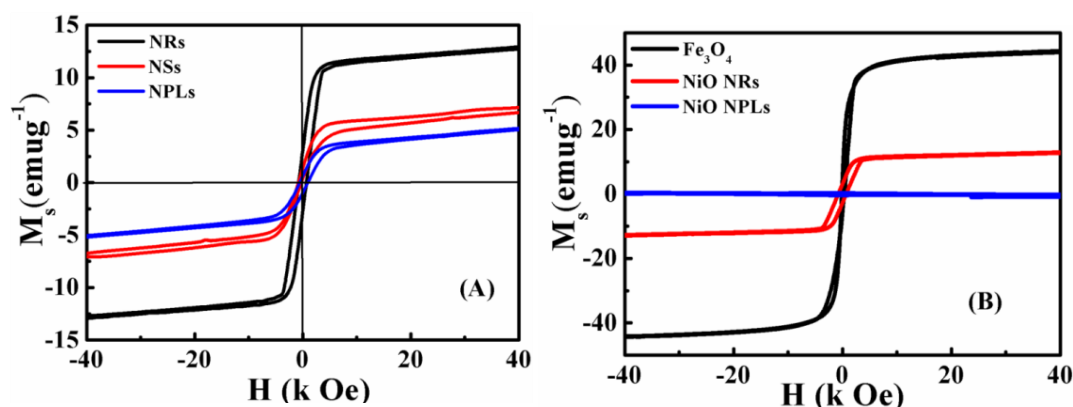
Figure S10.   Magnetization curves of NiO NRs, hexagonal NiO NPLs, and Fe_3O_4.

Supplementary S11
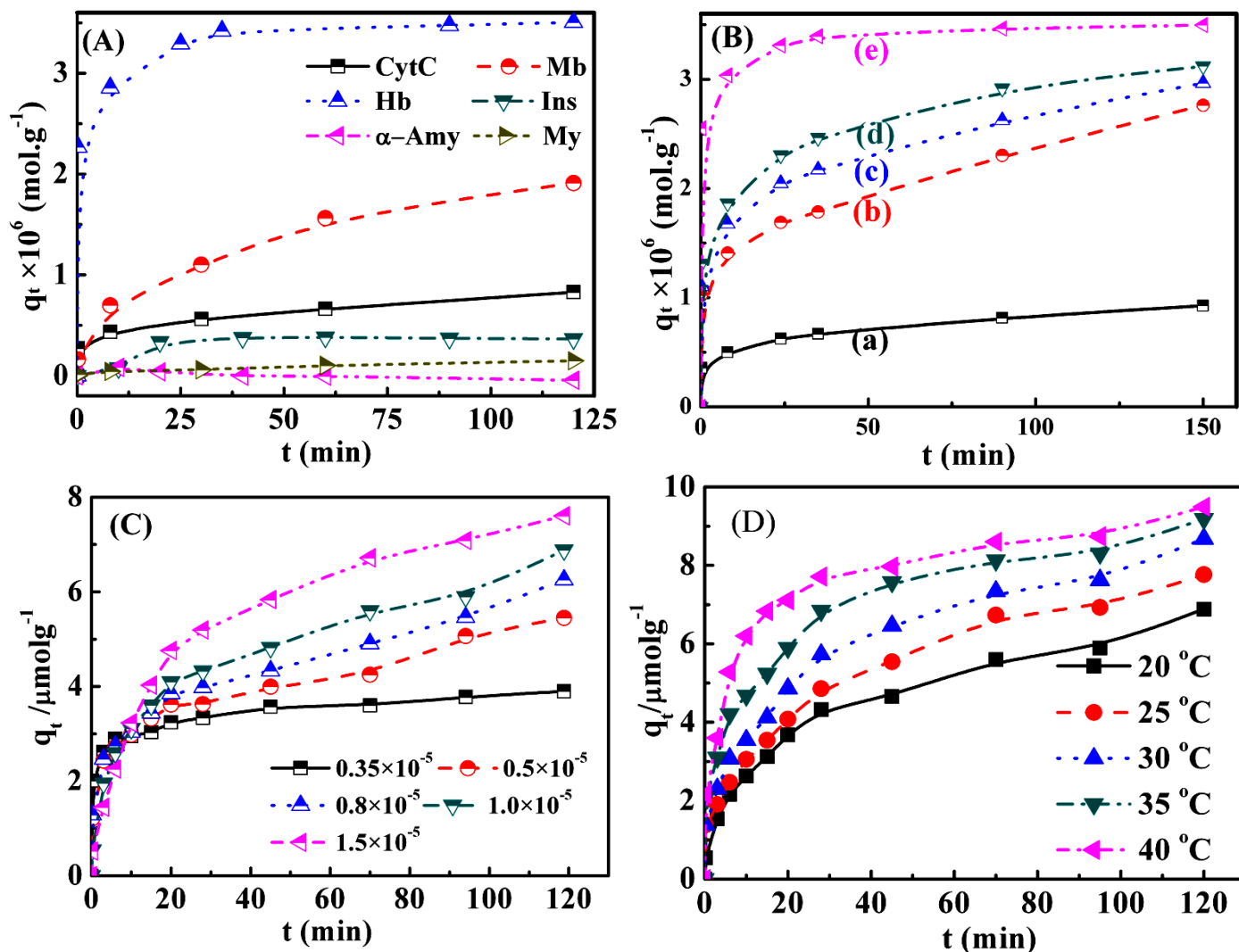
Figure S11. A) Time dependence of adsorption amount of 3.5×10^{-6} M proteins on mesoporous NiO NRs, B) Effect of chemical composition and morphology of nanobiosorbent on the adsorption of 3.5×10^{-6} M hemoglobin a) Fe_3O_4 NPs, b) NiO NPLs (hexagonal), c) NiO NPLs (rectangular), d) NiO NSs, and NiO NR-like morphology, C) Effect of hemoglobin concentration on the adsorption assays over 0.025 g NiO NRs, and D) The temperature effect of 1×10^{-5} M hemoglobin adsorption at NiO NRs structured.

Supplementary S12
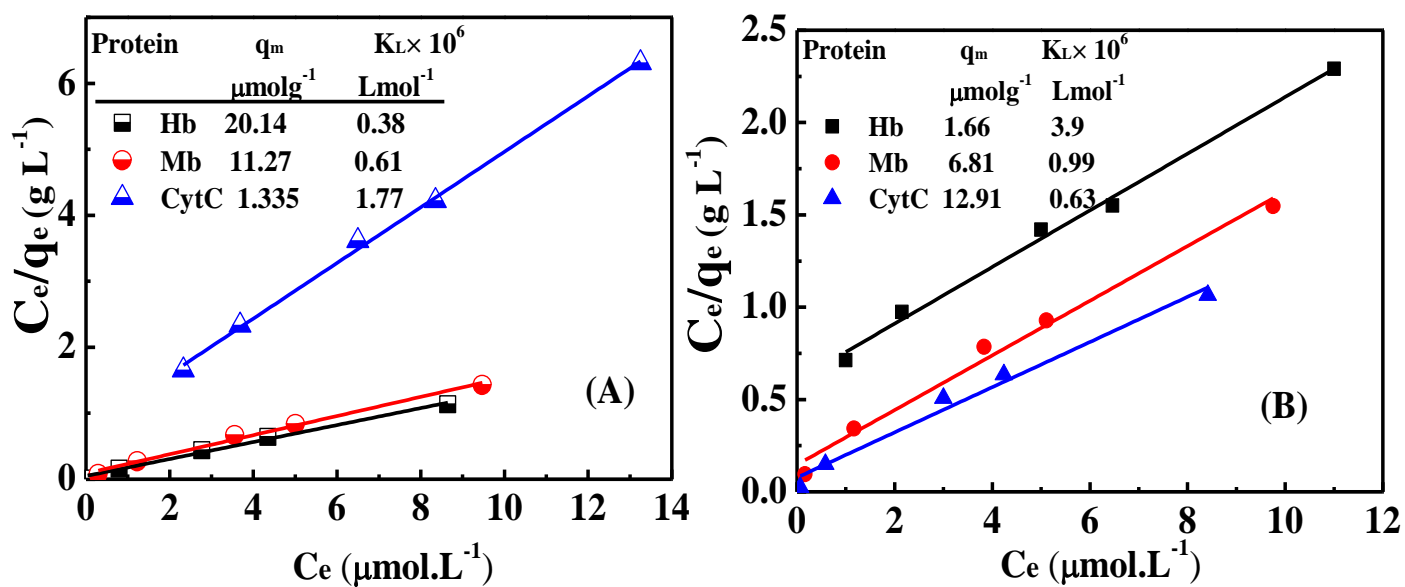
Figure S12 A) Langmuir adsorption isotherms of proteins at NiO NRs, B) adsorption assay of proteins over nanomagnet particles. B) Langmuir adsorption isotherms for adsorption of heme-proteins into 0.83 g/L of NiO NRs (A) and 0.83 g/L of Fe_3O_4 NPs (B)

20

Supplementary S13
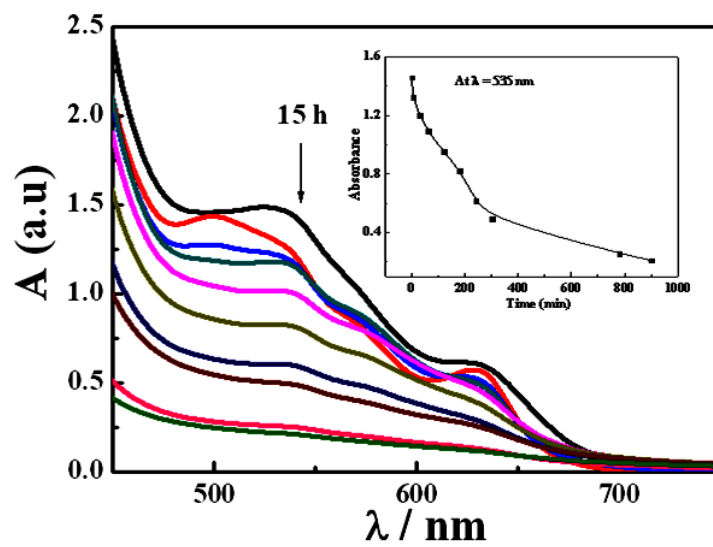
Figure S13. Adsorption of 6.06×10^{-4} M Hb at (0.833 g/L) mesoporous NiO NRs at 20 °C.

Supplementary **S14**
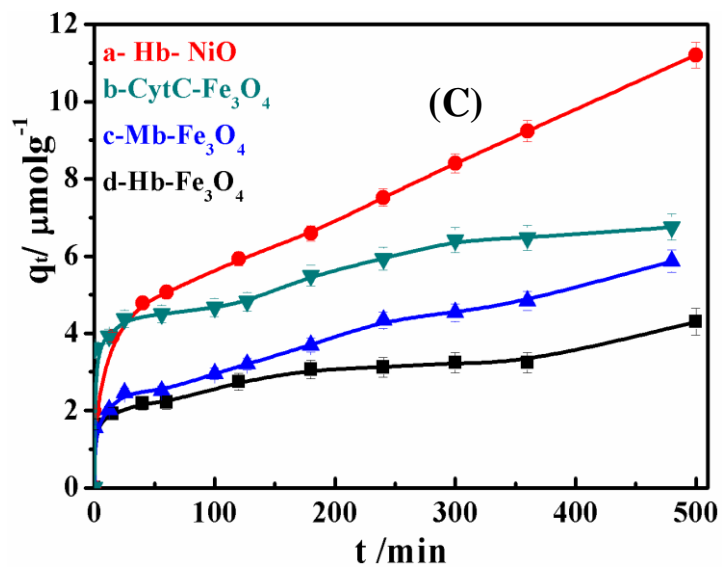
Figure S14 Adsorption affinity of $(1 \times 10^{-5}$ M) heme-protein cargos at Fe_3O_4 NPs compared with NiO NRs.

Supplementary S15

To understand the chemical behavior of the molecular adsorption characteristics of heme-proteins on NiO and Fe_3O_4 NMs, soft docking algorithm were implemented on SYBYL-X suite program (Scheme 1).[9] With respect to the NiO and Fe_3O_4 nanomagnets, the docking studies perform energy function calculations along the axial orientation of the interacting molecules in space. The energy function is represented in the form of force field that describes the bond, angle, and dihedral angle potentials. The molecular activity of surfaces was estimated from the orbital occupation point of view of NMs. Scheme 1 shows that the highest occupied molecular orbital (HOMO) is localized for both models of NiO and Fe_3O_4 NMs. It consists of pre-constructed solid cross-section surface of NiO and Fe_3O_4. These models were constructed based on previously reported space groups *Fm3m* and *Fd3m* for NiO and Fe_3O_4, respectively. In addition, two protein models CytC and Hb were used for docking. All atoms of the surfaces were constrained through the docking processes, preventing them from moving.

In general, Scheme 1 revealed that the selective and adsorbed protein might be encapsulated into the interior of the mesopores of NMs or bind between NPs (rose/sphere/or platelet), as previously reported Ref. 2c. To show evidence of the key factors of chemical interaction, and protein orientation and structural feature on the adsorption process, the adsorption free energy (ΔE_{ads}) was calculated from the equation ($\Delta E_{ads} = E_{comp} - (E_P + E_{Sur})$) to evaluate the stability of existing complex model, where E_{comp}, E_P, and E_{Sur} are the energy of solid-protein complex, protein, and solid, respectively (Scheme 1). Our results show that the geometrical NiO NMs occupied by parallel, unpaired spin electrons are concentrated in the lattice center. In turn, the

geometrical Fe_3O_4 NMs occupied by unpaired spin electrons are localized in the lattice terminals. These spin orientations of NMs may be responsible for surface magnetization. Moreover, protein-NiO complex interactions afforded high adsorption/immobilization stability (i.e. high negative value of adsorption free energy, E_{ads}), compared with Fe_3O_4 NMs surface adsorption. These results reveal that the selective adsorption affinity of heme-proteins, particularly Hb, is favorable with NiO than that of Fe_3O_4 NMs. These results also presented the practical method of heme-protein separation without intensive design and experimental conditions. These results also indicate that NiO NMs with specific morphology, such as NRs, can be engineered for selective applications, including enrichment and separation of proteins, as well as, drug delivery.

Supplementary S16

To study the stability and efficiency of the adsorption model, the adsorption of Hb was carried out in different temperatures ranging from 20 °C to 35 °C. Results show that the loading affinity of protein cargos increased with increasing temperatures. In addition, the kinetics and thermodynamic parameters of the adsorption assay were depicted (see Figs S14-S16). Furthermore, "pseudo-first-order" was used to describe adsorption in solid–liquid systems based on the adsorption capacity of nanomagnet solids to investigate the adsorption mechanism. The adsorption rate was in the following sequence Hb >>> Mb > CytC. The thermodynamic equilibrium constant K_c increased with increasing temperature, whereas the absolute value of ΔG decreased with increasing temperature. This result indicates that adsorption was spontaneous and more favorable at high temperature, confirming an endothermic adsorption process of protein immobilization.
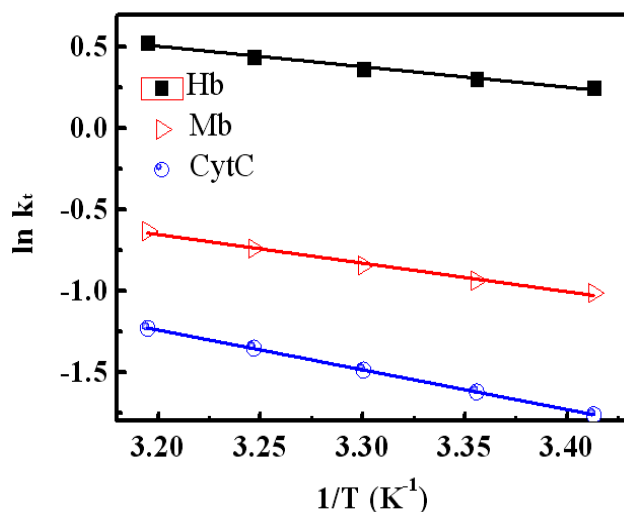
Figure S16. Effect of temperture on the adsorption rate constant of heme-proteins at NiO NRs.

Table S17. Thermoynamic and kinetic parameters of the adsorption of heme-proteins at NiO NRs.

Protein	T/K	k_t / s^{-1}	Kc	Ea/kJ mol^{-1}	ΔH$^{\#}$/kJ mol^{-1}	ΔS$^{\#}$/ J mol^{-1}K^{-1}	ΔG$^{\#}$/kJ mol^{-1}	ΔH/kJ mol^{-1}	ΔS/J mol^{-1}K^{-1}	ΔG/kJ mol^{-1}
Hb	20	0.032	1.147253				63.00			-0.335
	25	0.0339	1.188046				64.08			-0.427
	30	0.0359	1.337016	10.48	7.959	-215	65.15	-18.47	63.74	-0.732
	35	0.0389	1.554665				66.23			-1.13
	40	0.0423	1.842494				67.30			-1.59
Mb	20	0.0091	0.400877				61.84			2.227
	25	0.0098	0.469527				62.89			1.873
	30	0.0108	0.582649	14.62	12.099	-211	63.95	-28.97	91.11	1.361
	35	0.0119	0.680355				65.00			0.986
	40	0.0133	0.861966				66.06			0.387
CytC	20	0.0043	0.07945				58.03			6.169
	25	0.0049	0.091867				59.02			5.915
	30	0.0057	0.106965	20.34	17.818	-198	60.01	-33.31	92.08	5.631
	35	0.0065	0.138711				61.00			5.058
	40	0.0074	0.193534				61.99			4.274

Supplementary S18

Protein	k (rate of adsorption)
a- Hb	1.68×10^{-3}
b-My	0.14×10^{-3}
c- Cyt C	0.12×10^{-3}
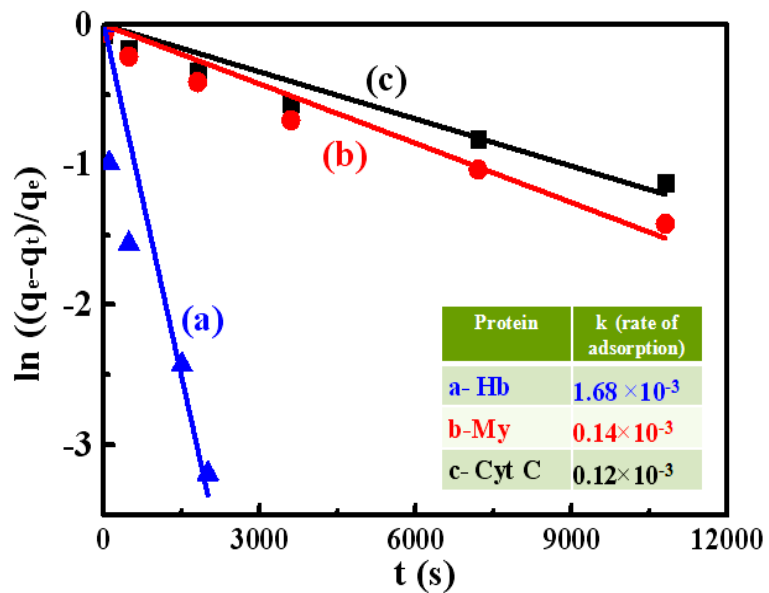
Figure 18. Integrated first order adsorption of heme-proteins over NiO NRs (inset the values of adsorption rate constant).

Supplementary S19

Based on the intra-particle diffusion theory, the uptake of adsorbate is proportional to the square root of contact time in the course of adsorption[3a]. The relation of q_t versus $t^{0.5}$ does not pass the origin, indicating that the diffusion in boundary layers involves mass diffusion at the external surface of the particles through the hypothetical boundary layers surrounding the particles due to particle morphology. Furthermore, the large intercept suggests that the process largely involves external surface adsorption (See Supplementary S17). The intra-particle diffusion was in the following sequence Hb >>> Mb > CytC, in agreement with k_t and Kc and q_t values of the protein adsorption over NiO NMs (Fig. S18-insert).

Protein	k (intraparticle diffusion rate)	C constant
Hb	0.02915	2.18353
Mb	0.01973	0.28617
CytC	0.00668	0.2673
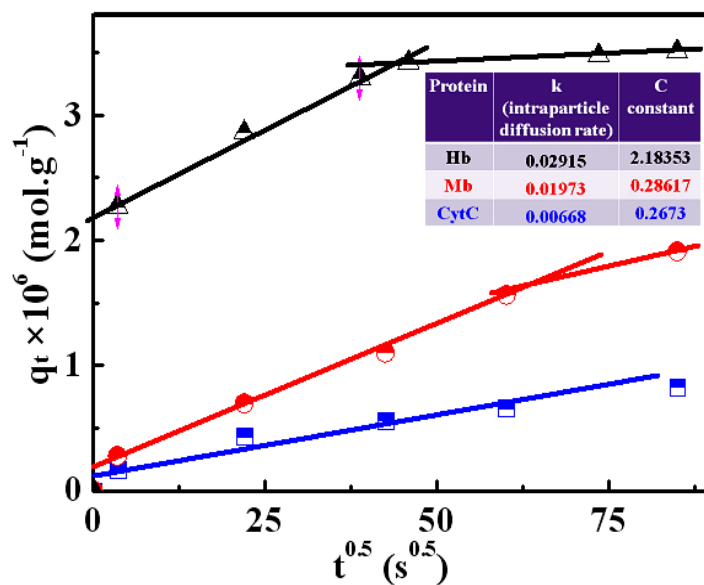
Figure S19. Intra-particle diffusion plot for heme-protein adsorption on mesoporous NiO NRs.

Supplementary S20

Reusability process of biosorbent NiO nanomaterials

After the first set of reaction experiments, a simple chemical treatment based on acidified solution (HCl/NaCl- pH 3) was used to effectively remove the trapped proteins adsorbed on mesoporous magnetic NiO non-materials without significant damage in the morphology and physical properties of the nanostructures. The precipitate was then collected and dried overnight at 60 °C.
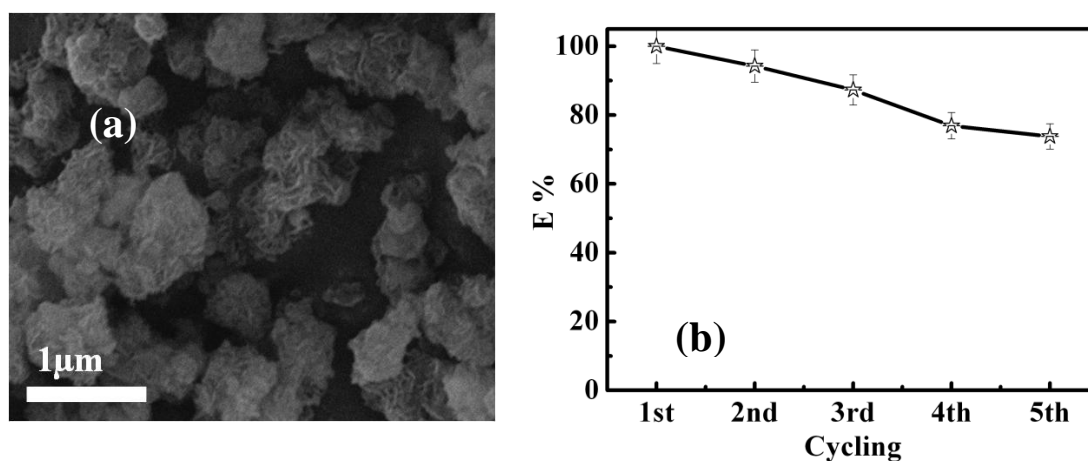
Figure S20. FE-SEM image of mesoporous NiO NRs after 3rd reuse cycle, b) Reusability study of NiO NRs during the adsorption of Hb from human blood up to five times. The efficiency of the nanofilter system (E) was calculated from the % ratio of adsorbed amount (XC) per reuse cycle (No.) and the initial adsorbed amount (X) obtained from the initial use of the NiO NRs.

Supplementary S21
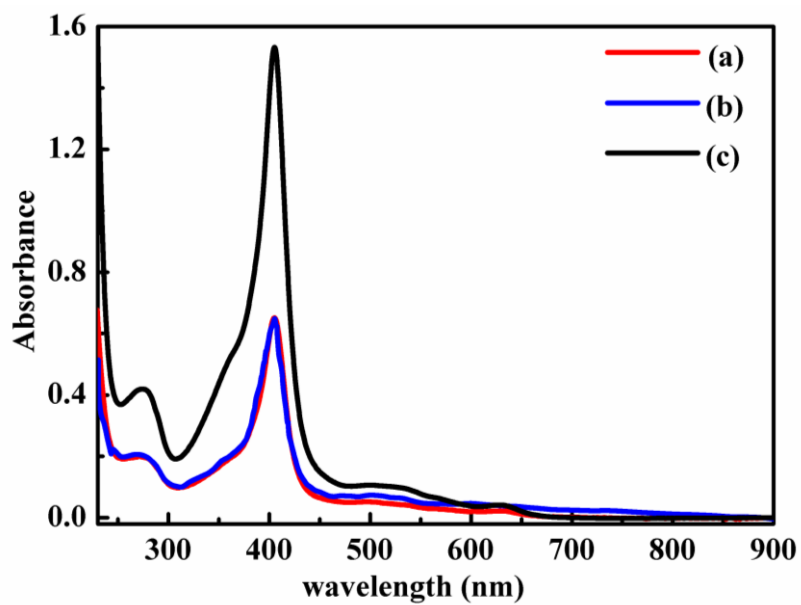
Figure S21. UV-vis spectrum of hemoglobin desorbed from the mesoporous NiO NFs. a) 10 μ M Hb in water, b) recycled Hb at pH 5, and d) recycled Hb at pH 2.